CORE AND EDGE TRANSPORT OF SCENARIO WITH INTERNAL TRANSPORT BARRIER IN TRITIUM AND DEUTERIUM-TRITIUM PLASMAS IN JET WITH BE/W WALL

[1]CF MAGGI, [1]M FITZGERALD, [1]H DUDDING, [2]J ERIKSSON, [1]S MENMUIR, [3]M NOCENTE, [1]C OLDE, [4]M PORADZINSKI, [5]I PREDEBON, [3]D RIGAMONTI, [1]I BALBOA, [1]C CHALLIS, [6]E DELABIE, [7]FA DEVASAGAYAM, [1]A FIELD, [8]E JOFFRIN, [1]D KING, [1]E LERCHE, [8]X LITAUDON, [1]E LITHERLAND-SMITH, [1]S SAARELMA, [1]Ž STANCAR, [7]T TALA, [1]I VOITSEKHOVITCH, JET Contributors* and EUROfusion Tokamak Exploitation Team[$]

[1]United Kingdom Atomic Energy Authority, Culham Campus, Abingdon, Oxfordshire OX14 3DB, United Kingdom of Great Britain and Northern Ireland; [2]Department of Physics and Astronomy, Uppsala Universitet, Uppsala, Sweden; [3]Dipartimento di Fisica, Universita' degli Studi Milano-Bicocca, Milan, Italy; [4]Institute of Plasma Physics and Laser Microfusion, Warsaw, Poland; [5]Istituto per la Scienza e Tecnologia dei Plasmi, CNR, Padova, I-35127, Italy; [6]Oak Ridge National Laboratory, Oak Ridge, TN 37831-6169, USA; [7]VTT, PO Box 1000, FI-02044 VTT Espoo, Finland; [8]CEA, IRFM, F-13108 Saint-Paul-lez-Durance, France
See the author list of CF Maggi et al. 2024 Nucl. Fusion **64 112012*
*[$]See the author list of E Joffrin et al 2024 Nucl. Fusion **64** 112019*

Email: Costanza.Maggi@ukaea.uk

Abstract. In view of ITER and future fusion reactors, where internal transport barriers (ITBs) may form spontaneously, there is a need to fully understand the physics of ITB trigger and sustainment in order to avoid it or control its strength. For the first time on JET with metallic wall, we reveal the importance of the main ion isotope mass on ITB physics (triggering and strength) by comparing a unique dataset of discharges performed in D, T and D-T. First principle calculations of the reduction of anomalous transport with different isotopes are provided to shed light on the underlying physics.

1. ITB SCENARIO IN JET WITH Be/W WALL: EXPERIMENTS IN D, T AND D-T

This paper reports on experiments performed in JET-ILW (Be wall and W divertor) to obtain plasma discharges at low density, n_e, (low plasma recycling conditions) and high core ion temperatures (T_i), with a strong internal transport barrier in plasmas with different main ion hydrogenic isotopes: D, T and D-T. Contrary to the JET D-T baseline and hybrid scenarios, aimed at maximum fusion power sustained for 5s [1], the D-T ITB scenario was intended to provide a suitable, albeit transient, target plasma for the observation of toroidal Alfvén Eigenmodes (TAEs) destabilized by fusion born α-particles. This measurement was achieved during the after-glow phase of the discharge, after NBI switch-off [2]. The JET-ILW ITB scenario was first developed in D plasmas [3] and subsequently tested in T plasmas for isotopic dependencies. It was then executed in plasmas with D-T mixtures in DTE2, with D-T gas injection and D-T NBI heating. Additional discharges were performed in the last JET D-T campaign, DTE3, with D-NBI heating into T-plasmas. Due to the limited amount of time devoted to this programme and its scientific focus on energetic particle physics, there was no emphasis on optimising the ITB scenario per se. As a result of this work, a unique dataset of plasmas with ITBs in D, T and D-T in JET with the metallic Be/W wall is available for studies of isotope mass dependence of ITB trigger and strength.

The electron and ion kinetic profiles of one of such discharges (JET pulse #96852, D) are reported in FIG 1, showing the presence of a strong ITB at mid radius in both ion and electron channel, in particular T_i and n_e. In JET with C wall (JET-C), a 'strong' ITB was defined in relation to a dimensionless figure of merit introduced by [4], $\rho^*_{Ti} = \rho_s/L_{Ti}$ (with ρ_s the ion Larmor radius and L_{Ti} the local ion temperature gradient scale length = $T_i/(\partial T_i/\partial R)$). Strong ITBs were classified as having $\rho^*_{Ti} > 1.5 \times \rho^*_{ITB}$ (with $\rho^*_{ITB} = 1.4 \times 10^{-2}$ the empirically found threshold value). This empirical criterion is found to be valid also for the dataset of JET-ILW ITB discharges of this study. n_e profiles were measured by High Resolution Thomson Scattering (HRTS) [5] or profile reflectometry [6] (depending on diagnostic availability), T_e profiles by ECE [7] and HRTS and T_i and toroidal angular rotation (Ω_{tor}) by core and edge charge exchange spectroscopy (CXRS) on Ne X impurity, via diagnostic Ne gas puffs [8]. Additionally, main ion core CXRS measurements are also available.

1.1 Main characteristics of the JET-ILW scenario with ITB

The main characteristics of the JET-ILW ITB scenario of this study are $B_T = 3.43$ T, $I_P = 2.8$ MA ($q_{95} \sim 3.8$), the lowest density achieved in JET-ILW at this I_P/B_T ($n_e \leq 4 \times 10^{19}$ m^{-3}), high core ion temperatures ($T_{i,core} \geq 10$ keV) and auxiliary heating from NBI only ($P_{NBI} = 22$ - 30 MW). FIG. 2 shows times traces of main plasma parameters for D-T pulse #99946. Since the presence of an extended region of low, positive magnetic shear, ŝ, in the plasma

core is known to favour triggering of ITBs when q_{min} reaches rational values [9], [10], [11], to obtain a central q-value $q_0 \sim 1.5$ the NBI heating was applied during the plasma current ramp-up phase to slow down the current profile diffusion [10]. The q-profile is reconstructed using a bespoke EFIT equilibrium constrained by kinetic pressure and fast ion pressure profile (computed by interpretative TRANSP [12] simulations) and benchmarked by MHD markers and polarimetry. The ITB is consistently found to form at the location of the plasma q = 2 surface, as illustrated in FIG 3. This finding applies to all pulses of the dataset, regardless of the main ion isotope mass.

The total neutron rate computed by interpretative TRANSP simulations is in good agreement with that measured by fission chambers once constrained by state-of-the-art neutron spectroscopy analysis, validating the core plasma fuel ratio. Time-of-flight (TOFOR diagnostic) measurements are used for D and T plasmas [13] and diamond detectors data for D-T plasmas [14]. The edge plasma isotopic ratio is measured by high resolution H, D, T Balmer-α spectroscopy of a Penning discharge within the neutral gas analysis diagnostic in the JET sub-divertor plenum [15]. After ITB onset, the thermonuclear (TH) contribution to the total neutron rate increases significantly, reaching up to 50-60% of the beam-target (BT) component in the D-T plasmas and ratios of TH /BT ~ 1 in the T pulses at peak neutron rate.

1.2 Motivation of the study: easier ITB onset and stronger ITB in Tritium plasmas

The motivation of this study is the observation that the main ion isotope mass has an impact on ITB access and strength: ITB onset is easier, namely occurs at lower NBI input power, in T plasmas and, once formed, the ITB is stronger in T plasmas than in D and D-T counterpart discharges. In the best performing ITB discharges of the dataset, the T pulse achieves an ITB with the highest core T_i and core Ω_{tor}, despite having the lowest NBI power (23 MW), compared to 26 MW in the D-T pulse and 31 MW in the D pulse. In FIG 4a we compare the ion and electron temperature profiles of the best performing pulses with ITB in D (#96852) and T (#99206), at the time of ITB onset (dashed lines) and strong ITB (solid lines). For both discharges, the time of strong ITB is 50 ms before NBI switch-off. The ion ITB foot is found at a larger radius in T than in D in the fully developed ITB phase. FIG 4b shows that the core ion heat diffusivity χ_i, computed by TRANSP, is lower for T than D and over a wider plasma volume, reaching neo-classical values (TRANSP + NCLASS). As the T pulses also have the lowest plasma density, in order to understand the physics at play it is necessary to decouple isotope mass effects from density effects on ITB trigger and strength.

1.3 Pacing pellets and ITB scenario with type III ELMy edge

An additional feature of the ITB scenario in JET-ILW was the use of high-field-side pellet pacing (~ 2 mm, 40-45 Hz pellets) to mitigate type I ELMs for W control, to prevent large W influxes into the core plasma from the pedestal region. We recall that ITBs are not compatible with type I ELMy pedestals, as reported in many tokamaks, e.g. [16]. D pacing pellets were used in D and D-T plasmas, while H pacing pellets had to be utilized in T plasmas, since T pellets were not available on JET (and D pellets were not allowed in T plasmas, due to 14MeV neutron budget constraints). As a consequence, the tritium ITB plasmas have a sizeable H concentration at the edge (~ 11-17%) and an effective isotope mass $A_{eff} \sim 2.8$. In fact, A_{eff} could be somewhat different at the pedestal, compared to the sub-divertor measurement, due to the high pellet efficiency there. A few discharges were performed in D with H pacing pellets, for comparison, and they are included in the pedestal analysis of Section 2. FIG 5 shows that the pellets request window starts at the time of the NBI power step to ~ 20 MW and the phase of pellet triggered ELMs (indicated by blue markers with value = 1 in the bottom panel of FIG 5) occurs in the discharge phase with large type I ELMs, since ELM triggering by pellets depends on pellet mass, speed and pedestal conditions [17]. In this phase, we observe a combination of natural and pellet-triggered type I ELMs. Subsequently, a clear transition to a phase with small/high frequency type III ELMs occurs, with decrease in edge density, where the pellets no longer trigger ELMs. The ITB forms and grows in this phase with reduced pedestal performance. We note that the cause-effect of this transition is not yet clear, namely whether the transition from type I to type III ELMy pedestal, due to a reduction in P_{sep}, triggers the ITB onset or whether the formation of a transport barrier at mid-radius reduces the power flux through the separatrix, leading to the transition from a type I ELMy pedestal to a type III ELMy pedestal, with lower $n_{e,PED}$ and $T_{e,PED}$. A similar picture is observed in both D and D-T plasmas.

The T plasmas, instead, evolve differently throughout the discharge. The H pellets request time window is identical to that in the D and D-T pulses, but the pellets do not trigger ELMs. The T plasmas transition into H-mode with type III ELMs and remain so for the entire duration of the NBI heated phase (see FIG 6). Indeed, the low-density plasmas of our study access H-mode from the low density branch of P_{L-H}, where the power

threshold is very high [18]. As the discharge progresses in time, the power through the separatrix, P_{sep}, after reaching a maximum value at maximum P_{NBI}, decreases in time due to the (moderate) increase in bulk radiation (see top panel of FIG 6), thus the plasma falls even 'deeper' in the type III ELMy regime. The edge density strongly decreases in time, and the ITB forms in this phase. After ITB onset, the density profile becomes very peaked, due to a sizeable reduction in pedestal density and increase in core density. In the low recycling conditions typical of these plasmas, the phase prior to the L-H transition carries an important legacy for the subsequent, high-power phase of the discharge. This is clearly exemplified by a pair of discharges at similar P_{NBI} ~ 25 MW and injected gas rate ~ 5 x 10^{21} e/s, but with different P_{NBI} and gas waveforms before the L-H transition. T pulse #99198 has a gradual P_{NBI} increase and lower gas injection (thus lower NBI fuelling and gas fuelling), has very low density and transitions into H-mode with type III ELMs. It thus remains at low density throughout and eventually forms an ITB. Conversely, the D pulse (#97770) has an earlier L-H transition due to the higher P_{NBI} (and thus larger NBI fuelling) and higher gas injection rate. It transitions to a type I ELMy H-mode and thus naturally evolves to higher plasma density and does not trigger an ITB.

2. ISOTOPE MASS DEPENDENCE OF LOW-DENSITY PEDESTALS WITH TYPE III ELMs

In the plasma phases with type III ELMs, the pedestal top density, $n_{e,PED}$, decreases with A_{eff} from D to T, as shown in FIG 7 for a subgroup of the dataset with similar P_{NBI} = 23.5-26.5 MW. This is opposite to what is observed in type I ELMy H-modes, where $n_{e,PED}$ increases with A_{eff} [19], [20], likely due to a reduction in inter-ELM particle transport with increasing main ion isotope mass. The trend of decreasing $n_{e,PED}$ with A_{eff} is consistent with a strong contribution of neutral fuelling in setting the pedestal density structure in low recycling conditions, where neutrals with same energy but different isotope mass have a mean free path that scales as $1/\sqrt{A}$. This is corroborated by analysis of the pedestal density width, Δ_{ne}, which is found to be narrower in T than in D in the same dataset of low-density plasmas with type III ELMs. We recall that, instead, in type I ELMy H-mode pedestals Δ_{ne} does not vary with A_{eff} from D to T [19], while a steepening of the pedestal density gradient is observed from D to T, accounting for the increase in $n_{e,PED}$ with A_{eff} in those conditions.

As both neutral fuelling and particle transport contribute to setting the inter-ELM pedestal density structure, the latter also requires investigation. To this end, gyrokinetic (GK) simulations, with the code GENE [21], of the low-density type III ELMy pedestal of the ITB scenario are on-going, to identify the dominant micro-instabilities at play and assess the isotope dependence of pedestal heat and particle transport in these conditions. Initial, local, linear electromagnetic simulations have been carried out at three pedestal radial locations, top (ψ_N = 0.91), mid-gradient region (ψ_N = 0.97) and pedestal foot (ψ_N = 0.98), with 3 plasma species (electrons, main ions and Be impurities, with same dilution as for the case with the actual impurity mixture in experiment, namely Be + Ni + W) starting from the equilibrium of T ITB pulse #99206. With increasing wavenumber $k_y\rho_i$, the dominant micro-instabilities are found to be micro-tearing modes (MTM), Trapped Electron Modes (TEM) / Ubiquitous Modes (UM) and Electron Temperature Gradient Modes (ETG). Neoclassical transport is found to be negligible. GENE non-linear simulations are in progress. The pedestal stability of the low-density type III ELMy plasmas is analysed with linear, ideal MHD stability with the Helena/ELITE codes [22], [23]. As expected for these conditions, the operating point is found to be deeply stable to ideal peeling-ballooning modes.

In summary, in the low-density plasmas with type III ELMy edge, the T plasmas evolve to lower pedestal density. This has important consequences for the core transport properties in the discharge phase with ITB, as addressed in the following section.

3. ISOTOPE DEPENDENCE OF ITB TRIGGER AND STRENGTH

It has long been known that several physical effects are key to ITB triggering and strength. They are linked to stabilization of the dominant core plasma turbulence. In JET, with dominant NBI heating, the dominant core micro-instabilities are typically Ion Temperature Gradient (ITG) modes. Work in JET-C had shown that the q = 2 and q = 3 surfaces play a major role in the formation of ITBs in plasmas with low, positive magnetic shear $\hat{s}$ = r/q dq/dr [9], [10], [11]. More recently, [24] have shown with local, nonlinear GK simulations, that turbulent eddies can extend in tokamak plasmas along magnetic field lines for hundreds of poloidal turns when $\hat{s} \sim 0$ and that the eddies' self-interaction can strongly reduce transport. This mechanism is put forward as a potential explanation of why ITB trigger is easier in the vicinity of q = rational surfaces.

An important mechanism for stabilizing ITG turbulence is ExB shearing [25], [26], which was shown to play a major role in JET-C ITBs [27]. Here we define the ExB shearing rate as $\omega_{ExB} = | R B_\theta/B_\phi \, \partial/\partial r \, (E_r/RB_\theta) | \, (s^{-1})$, with E_r defined by the equation for radial force balance, $E_r = 1/(Ze\, n_i) \, \partial p_i/\partial r - v_\theta B_\phi + v_\phi B_\theta$. For plasmas with

dominant NBI heating, which is the case of the discharges of this study, a major role is played by the external momentum input, with the (v_ϕ B_θ) term as the driving term. In addition, in the phase with fully developed ITB the diamagnetic term of E_r also plays a role in the quantification of ω_{ExB} due to the strong pressure gradient.

ITG modes are also known to be stabilized by increasing values of T_i/T_e. For the low-density plasmas with ITB and type III ELMy edge of this study, we expect the ion-electron coupling to be weak, $P_{e\text{-}i} \sim Z^2/m_i$ ($n_e n_i/T_e^{1.5}$) (T_e-T_i), as indeed confirmed by TRANSP power balance. Furthermore, as $P_{e\text{-}i}$ is inversely proportional to the isotope mass, we also expect larger T_i/T_e for the T plasmas, with lower n_e and higher isotope mass.

Stabilization of ITG modes by fast ions, via dilution and/or pressure, has been shown to be an important player in ITBs, on certain tokamaks, e.g. on AUG [28]. As discussed in the next section, this mechanism is not a major player in the JET-ILW ITB plasmas analysed. The fast ion dilution in the plasma core, n_{FI}/n_i, varies between ~ 15-25 % at ITB onset and ~ 10-20% in the phase with fully developed ITB, as derived by TRANSP interpretative simulations. There is no significant variation in n_{FI}/n_i amongst the D, T or D-T plasmas considered. A recent experimental study and comparison with GK (GENE) simulations of the isotope dependence of core heat transport in JET-ILW D vs T plasmas shows a reduction in T_i stiffness with increasing hydrogenic isotope mass, which is attributed to increased thermal electromagnetic (EM) stabilization of ITG turbulence with increasing isotope mass [29]. We therefore explore also this effect, as part of the core GK analysis presented in section 3.2.

A series of GK simulations have been carried out with the code CGYRO [30], starting from the equilibria of selected D and T discharges, to understand the impact of isotope mass on ITB trigger and strength, as well as the roles of magnetic shear, toroidal rotation shear, T_i/T_e, fast ions and thermal EM stabilization. Prior to this, we need to identify any potential impact of density on the q-profile and its shear in the JET-ILW plasmas with ITB. The main findings of this analysis are presented in the next section.

3.1 Impact of density scan on magnetic shear in plasma with ITB

In this section we assess whether variations in plasma density affect the q-profile of JET-ILW plasmas with ITB. We already established in Section 1.1 that the ITB foot is located at the plasma q = 2 surface, regardless of the main ion isotope mass. To this end, we analyse a systematic density scan carried out in the early phase of the hybrid scenario with performance overshoot [31], at I_P/B_T = 2.1 MA/3.45 T and D plasma, generating high core and edge T_i [32]. The plasma density was varied at H-mode entry from pulse to pulse, over eight discharges at same P_{NBI} = 29 MW, via variation of gas level or timing. While the density variations strongly affect core and edge T_i and core Ω_{tor}, they have a negligible impact on ŝ in this early phase of the pulse. Core (and edge) T_i and Ω_{tor}, as well as ITB strength, all increase with decreasing density. From the large increase in core Ω_{tor} at lower density we expect stronger ExB shear stabilization of core turbulence in these conditions.

Analysis of MHD spectra from the Mirnov pick-up coils reveals an n = 1 MHD mode appearing at the same time in all 8 pulses, regardless of density. The n = 1 mode is identified as being a rotating island**,** rotating with similar frequency f_{MHD} ~ 10-15 kHz in all 8 pulses. As magnetic islands form where the magnetic tension vanishes, for $k_\parallel \sim (m - nq) = 0$ with m and n integers and n = 1, q must also be integer for $k_\parallel$ to vanish. By relating the MHD mode frequency to the plasma toroidal rotation frequency ($f_{MHD} \sim n\, \omega_{tor} / 2\pi$), we pinpoint the radial location of the q = 2 surface, which coincides with the ITB foot location (R_{mag} ~ 3.6 m), for all 8 pulses regardless of density. This indicates that the q-profile is very similar in all 8 pulses in the early phase of the discharge with performance overshoot, and that ŝ is largely independent of plasma density variations in the phase leading to ITB formation. We thus conclude that while a favourable q-profile with low, ŝ > 0 and q = 2 surface is necessary for ITB onset, it is not a sufficient condition for developing a strong ITB.

3.2 Core gyrokinetic analysis

We have so far assumed that the dominant micro-instabilities in the core plasma of the JET-ILW ITB scenario are ITG modes. In this section we confirm this assumption by means of GK simulations with the code CGYRO. Next, we report the key results from a series of linear GK simulations assessing ITG turbulence stabilization by magnetic shear, T_i/T_e, fast ions and thermal EM effects, as well as non-linear simulations assessing mode stabilization by ExB shear and Mach-number for varying main ion isotope mass.

Linear, flux tube GK simulations confirm that ITGs are the dominant micro-instabilities in the core plasma of the JET-ILW ITB scenario, both before and after ITB onset. This finding is confirmed by scans in a/L_{Ti}, a/L_{Te}

and a/L_{ne}. The simulations were carried out at three radial locations, ρ_{tor} = 0.4, 0.55 and 0.7 for the equilibria of D pulse #96852 and T pulse #99206. The isotope mass dependence is in line with the gyro-Bohm dependence of ITG turbulence scaling as $1/\sqrt{A}$, verified with a scan in T (/D) concentration in the D (/T) pulse. The linear growth rates peak at $k_y\rho_{unit}$ = 0.3, thus all linear scans are carried out at this value ($\rho_{unit} = \sqrt{(m_D T_e)}/(B e)$). A scan in magnetic shear, with ±50% variation from the experimental value $\hat{s}_{exp}$, confirms that stabilization of ITG modes for decreasing ŝ is an important effect for these plasmas. The stabilizing effect is present at all three flux tubes and both at ITB onset and in the fully developed ITB phase. Furthermore, trends with ŝ with or without fast ions included are very similar. GENE simulations on the same equilibria find similar trends.

Local, linear GK simulations with comparative broad scans in T_i/T_e for the D pulse (ρ_{tor} = 0.43) and the T pulse (ρ_{tor} = 0.47) confirm stabilization of ITG modes by increasing T_i/T_e. However, stronger ITGs stabilization by T_i/T_e is found for the T case at fully developed ITB, as shown in FIG 8. As discussed earlier, the T plasma, with lower density and higher isotope mass, is characterized by much weaker ion-electron coupling, both at ITB onset (T_i/T_e ~ 1.5) and at fully developed ITB (T_i/T_e ~ 2.2) compared to the D plasma (T_i/T_e ~ 1.2 and ~ 1.3, respectively).

Inclusion of NB fast ions leads to stabilization of core ITG modes, primarily due to dilution effects. The separate roles of fast ion dilution and pressure gradient on ITG stabilization was assessed with additional linear GK runs. Overall, the impact of fast ions on ITG modes is modest for the D and T ITB pulses considered, yielding a maximum variation of ± 20% in growth rate when the fast ion density is scanned by ± 40% of the value derived with TRANSP interpretative simulations.

Contrary to what reported by [29], we do not observe any impact of isotope mass on thermal EM stabilization of ITGs in the core of ITB shots #96852 (D) and #99206 (T). This result was obtained with linear simulations at ρ_{tor} = 0.43 (/ 0.47) for the D (/ T) equilibrium and β_e scans, and by changing the ion mass from D to T (/ T to D). The experiment is seen to be close to a mode transition, currently under investigation.

Non-linear CGYRO simulations reveal the major role played by ExB shearing in regulating ITG turbulence. A scan in ExB shearing rate, $\gamma_E = \omega_{ExB} / (c_{s,D}/a)$, and Mach-number is performed for the GA-standard case and varying the main ion isotope mass from H to D to T (see FIG 9). The GA standard case has similar gradients to those of the JET-ILW pulses at ITB onset (a/L_{ne} ~ 1 and a/L_T ~ 3) and the variations in γ_E (from 0.0 to 0.3) and Mach-number (from 0.0 to 1.0) encompass the experimental ranges: γ_E ~ 0.2-0.3 and Mach ~ 0.5-0.8. As shown in FIG 9 from top left to bottom right panel, the normalized heat flux decreases with increasing γ_E, in particular for the ion channel, and the isotope mass dependence reverses with increasing γ_E, leading to a stronger reduction in heat transport in T, consistent with the experimental observations. Furthermore, the high Mach-numbers in experiment exacerbate the isotope dependence of ITB onset and strength, favouring the T plasmas.

4. CORE W TRANSPORT IN THE JET-ILW SCENARIO WITH ITB

Core impurity transport studies in plasmas with ITB in JET-C had reported core impurity accumulation due to dominant neoclassical (NC) impurity transport inside the ITB, where turbulent transport is stabilized [33], [34]. Impurity peaking increased with impurity charge (C, Ne, Ni) and was ascribed to an inward particle pinch inside the ITB radius.

For the JET-ILW ITB scenario plasmas, we have studied core W NC transport with the drift kinetic code NEO [35] for T ITB pulse #99206. Intrinsic impurities are Be, W and Ni. In the simulations, W is treated as trace impurity, with Be and Ni as non-trace impurities, due to their sizeable concentrations. We found that impurity-impurity collisions are important in these plasmas and need to be retained for accurate core W transport predictions. Conversely, simplified NC transport approximations (such as FACIT [36]) yield predictions contrary to the experimental trend. The complex interplay of high Mach number (M_ϕ ~ 0.6), enhancing impurity screening at low plasma collisionality, but enhancing inward convection with increasing Z_{eff} (/ increasing collisionality), regulates the high and mid-Z impurity dynamics. The W and Ni density profiles initially peak at the low-field-side (LFS) of the tokamak and are flat or even hollow at the plasma centre. In the NBI-heated phase of the plasma discharge, as the ITB progressively grows in strength, the W and Ni radiation profiles maxima move radially inwards. Core W accumulation is predicted by NEO in the phase with strong ITB, due to weakening of W outward convection v_W after the ITB is formed (see FIG 10). This is due to stronger ∇n_i effects on NC transport than the screening ∇T_i effects ($V_{NC} \sim (C_{TS} (R/L_{Ti}) - R/L_{ni})$, with $C_{TS} = - H_Z/K_Z$). However, despite core W density peaking with strong ITB, the total radiated power remains low (P_{rad} ~ 6 MW, compared

to P_{NBI} ~ 23 MW) until NBI switch-off and the electron temperature profile is peaked, likely due to the beneficial edge conditions with small/high frequency type III ELMs moderating W influx through the pedestal.

5. CONCLUSIONS

Strong internal transport barriers have been achieved transiently in JET-ILW in a low-density scenario with NBI only, with low, positive magnetic shear and q = 2 surface and with type III ELMy edge in D, T and D-T plasmas. The ITB scenario was designed and executed only to enable physics studies of α-driven TAEs in D-T and not in view of optimizing the scenario itself in terms of sustained performance. Despite the limited experimental time devoted to this scenario, the unique dataset collected has allowed unravelling the origins of the isotope mass dependence of ITB onset and strength in JET-ILW. Easier ITB onset - at lower P_{NBI} - and stronger ITB is observed in T plasmas, favoured by the combination of multiple effects: i) optimal entry into H-mode with type III ELMs (plasma remains at low density throughout the entire phase with NB heating); ii) $n_{e,PED}$ decreasing with A_{eff} in low recycling conditions (leading to higher core toroidal rotation); iii) stabilization of core ITGs by T_i/T_e increasing with A_{eff} and with decreasing density; iv) larger decrease in core heat transport due to ExB shear stabilization of core ITGs for larger A_{eff} and larger Mach number (the latter favoured by lower plasma density). While W and Ni radiate at the tokamak LFS at the time of ITB onset, NEO simulations of core W NC transport predict core W impurity accumulation in the discharge phase with fully developed ITB (strong density peaking, low collisionality, high Mach-number), due to NC inward convection inside the ITB. Due to the sizeable concentrations of Be and Ni impurities in these plasmas, the effect of impurity-impurity collisions cannot be neglected in the core W transport prediction. This precludes the use of simplified NC transport approximations, which yield predictions contrary to the experimental trend. Despite core W density peaking with strong ITB, the total radiated power remains low and the T_e profile is peaked until NBI switch-off, likely due to the beneficial edge conditions with type III ELMs moderating W influx through the pedestal.

ACKNOWLEDGEMENTS

This work has been carried out within the framework of the EUROfusion Consortium, funded by the European Union via the Euratom Research and Training Programme (Grant Agreement No 101052200 — EUROfusion). Views and opinions expressed are however those of the author(s) only and do not necessarily reflect those of the European Union or the European Commission. Neither the European Union nor the European Commission can be held responsible for them. (Please mind the addendum 2019-2020). This work has been funded by the EPSRC Energy Programme [grant number EP/W006839/1]. To obtain further information on the data and models underlying this paper please contact PublicationsManager@ukaea.uk. For the purpose of open access, the author has applied a Creative Commons Attribution (CC BY) licence to any Author Accepted Manuscript version arising.

REFERENCES

[1] MAGGI CF et al., Nucl. Fusion **64** (2024) 112012
[2] FITZGERALD M et al., Nucl. Fusion **63** (2023) 112006
[3] DUMONT R et al., Nucl. Fusion **58** (2018) 082005
[4] TRESSET G et al. Nucl. Fusion **42** (2002) 520
[5] PASQUALOTTO R et al., Rev. Sci. Instrum. **75** (2004) 3891
[6] MORALES RB et al., Rev. Sci. Instrum. **95** (2024) 043501
[7] DE la LUNA E et al., Rev. Sci. Instrum. **75** (2004) 3831
[8] HAWKES N et al., Rev. Sci. Instrum. **89** (2018) 10D113
[9] GORMEZANO C et al., Phys. Rev. Lett **80** (1998) 5544
[10] CHALLIS C et al., Plasma Phys. Control Fusion **43** (2001) 861
[11] JOFFRIN E et al., Nucl. Fusion **43** (2003) 1167
[12] PANKIN AY et al., Comput. Phys. Comm. **312** (2025) 109611
[13] VINGREN B et al., Nucl. Fusion **65** (2025) 096025
[14] RIGAMONTI D et al., Nucl. Fusion **64** (2024) 016016 & NOCENTE M et al., Rev. Sci. Instrum. **93** (2022) 093520
[15] VARTANIAN S et al., Fusion Eng. Des. **170** (2021) 112511
[16] SÖLDNER FX et al., Nucl. Fusion **39** (1999) 407
[17] CHAPMAN IT et al., Plasma Phys. Control. Fusion **58** (2015) 014017
[18] DELABIE E et al., APS Conference 2016
[19] FRASSINETTI L et al., Nucl. Fusion **63** (2023) 112009
[20] SCHNEIDER P et al., Nucl. Fusion **63** (2023) 112010
[21] JENKO F et al., Phys. Plasmas **7** (2000) 1904 & GÖRLER T et al., J. Comput. Phys. **230** (2011) 7053
[22] HUYSMANS GTA et al., 1991 Proc. CP90 Conf. on Computational Physics vol 2 p 371
[23] WILSON HR et al., Phys. Plasmas **9** (2002) 1277 & SNYDER PB et al., Phys. Plasmas **9** (2002) 2037
[24] VOLČOKAS A et al., Nucl. Fusion **63** (2023) 014003
[25] HAHM TS and BURRELL KH, Phys. Plasmas **2** (1995) 1648
[26] ERNST DR et al., Phys. Rev. Lett. **81** (1998) 2454
[27] TALA T et al., Plasma Phys. Control. Fusion **43** (2001) 507
[28] TARDINI G et al., Nucl. Fusion **47** (2007) 280
[29] BRIOSCHI D et al., Nucl. Fusion **65** (2025) 026054

[30] CANDY J et al., J. Comput. Phys. **324** (2016) 73
[31] HOBIRK J et al., Nucl. Fusion **63** (2023) 112001
[32] KING D et al., subm. Plasma Phys. Control. Fusion
[33] CHEN H et al., Nucl. Fusion **41** (2001) 31
[34] DUX R et al., Nucl. Fusion **44** (2004) 260
[35] BELLI EA and CANDY J, Plasma Phys. Control Fusion **50** (2008) 095010 and Plasma Phys. Control Fusion **54** (2012) 015015
[36] FAJARDO D et al., Plasma Phys. Control. Fusion **65** (2023) 035021

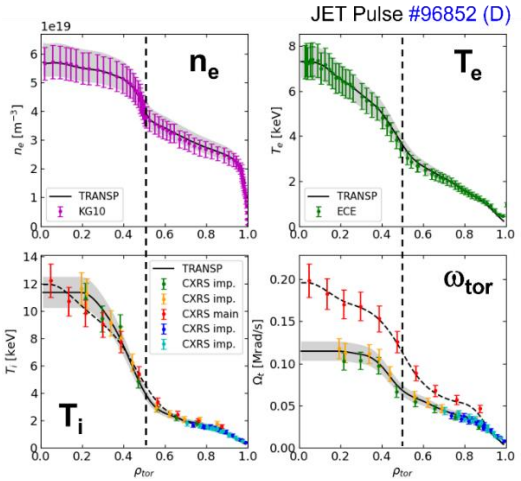

FIGURE 1. Ion and electron kinetic profiles for JET-ILW pulse #96852 (D) at t = 6.5 s (time of fully developed ITB). A strong ITB is observed in both ion and electron channels.

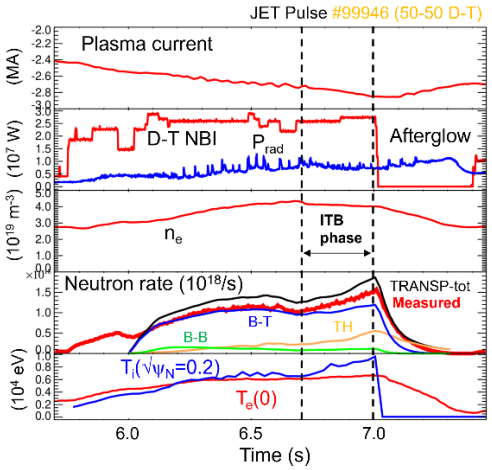

FIGURE 2. Time traces of main plasma parameters of JET-ILW ITB #99946, with 50-50 D-T.

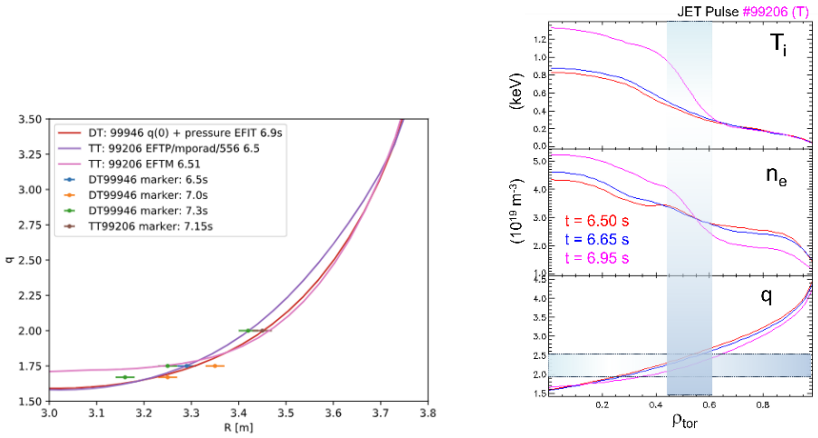

FIGURE 3. Left: q-profiles of ITB pulses #99946 (D-T) and #99206 (T) with overlayed MHD markers; **Right:** T_i, n_e and q-profiles of T ITB pulse #99206: t = 6.5s is the time of ITB onset, t = 6.95 s is the time of fully developed ITB (50 ms before NBI switch-off).

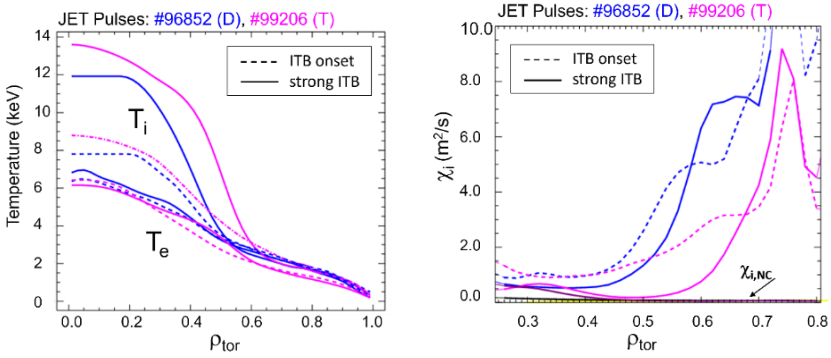

FIGURE 4-right. Comparison of power-balance core ion heat diffusivity (TRANSP) for JET-ILW ITB shots #96852 (D - blue) and #99206 (T - magenta) and neoclassical value $\chi_{i,NC}$ (TRANSP/NCLASS).

FIGURE 4-left. Ion and electron temperature profiles for JET-ILW ITB shots #96852 (D - blue) and #99206 (T - magenta). Dashed line: time of ITB onset; solid line: fully developed ITB.

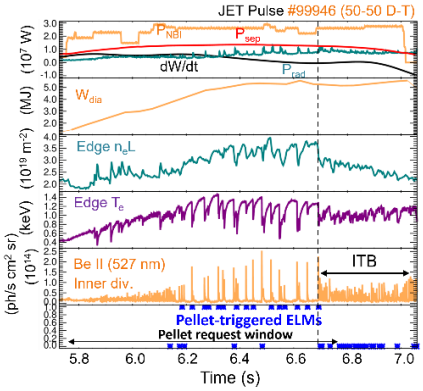

FIGURE 5. 50-50 D-T shot #99946 illustrates the transition from a phase with pellet paced, 'large ELMs' and no ITB to a phase with small/ high frequency type III ELMs and ITB.

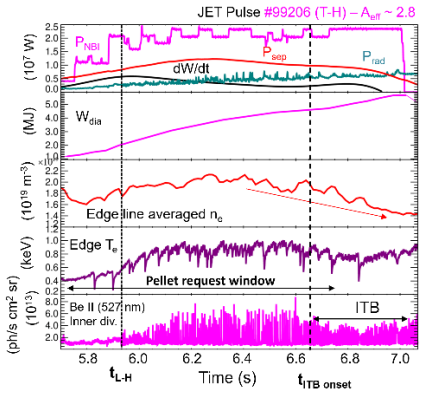

FIGURE 6. Time evolution of main parameters of JET-ILW ITB shot #99206 in tritium.

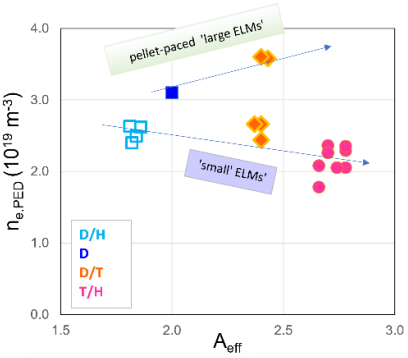

FIGURE 7. $n_{e,PED}$ of plasmas with type III ELMs decreases with A_{eff}. Arrows are to guide the eye only. Dataset at 2.8MA/3.43T, P_{NBI} = 23.5 – 26.5 MW, similar gas injection rates.

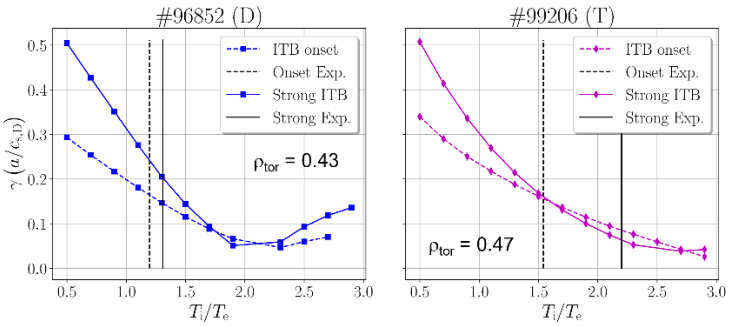

FIGURE 8. ITG growth rate (at $k_y\rho_i$ = 0.3) vs T_i/T_e from CGYRO linear simulations for D pulse #96852 (left) and T pulse #99206 (right).

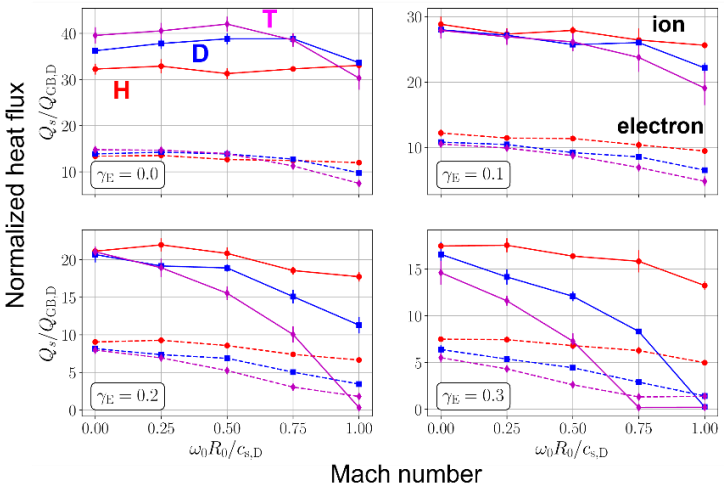

← **FIGURE 9.** Normalized ion (solid lines) and electron (dashed lines) heat fluxes vs Mach-number from NL CGYRO simulations on the GA-standard case. The normalized ExB shearing rate γ_E increases from 0.0 to 0.3 from top left to bottom right panel. H (red), D (blue), T (magenta).

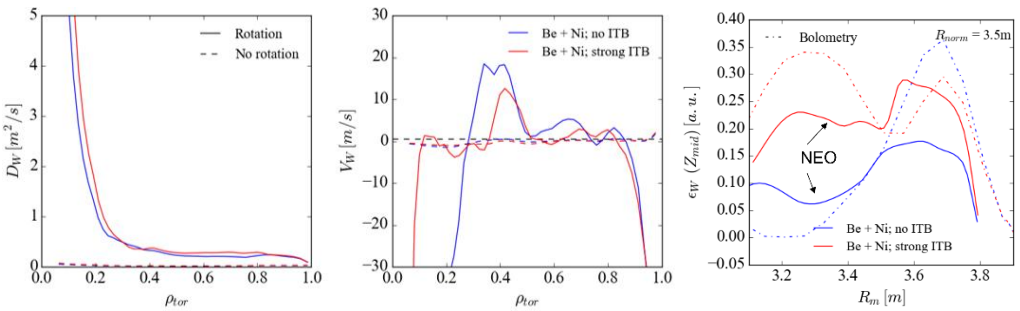

FIGURE 10. W diffusion coefficient (left) and pinch velocity (centre) from NEO predictions of core W transport for pulse #99206 in the phase of no ITB (blue) and strong ITB (red). Right: NEO prediction of W emissivity profiles (solid lines) compared to total radiation profiles (bolometry tomographic reconstruction). NEO profiles are normalized at R = 3.5 m.